

# Dielectric Polarisation In Partially Saturated Shales

*Paul R.J. Connolly<sup>1</sup>, Matthew Josh<sup>2</sup>, Keelan O'Neill<sup>1</sup>, Eric F. May<sup>1</sup>, Michael L. Johns<sup>1</sup>*

<sup>1</sup>Department of Chemical Engineering, M050, The University of Western Australia, 35 Stirling Highway, Crawley WA 6009, Australia.

<sup>2</sup>CSIRO Energy, ARRC Laboratories Kensington, Perth 6151, WA, Australia.

**Abstract.** Dielectric measurements of reservoir rocks are used to estimate important petrophysical properties such as water filled porosity and pore surface textures. However, complex dielectric polarisation processes that occur in rocks are strongly dependent on frequency, making physically meaningful interpretation of broadband dielectric data difficult. Here we demonstrate the application of Tikhonov regularisation methods to compute dielectric relaxation time distributions from broadband (40Hz to 110MHz) dielectric data for a shale sample at varying partial saturation. Furthermore, via the Kramers-Kronig relation the contribution from in phase conduction currents to the imaginary component of the dielectric response was quantified. The evolution of dielectric polarisation processes with increasing moisture content was analysed directly from changes in relaxation time distributions. It was found that the dominant polarisation mechanism up to a critical partial saturation occurred exclusively in the electrical double layer (EDL). Above this critical partial saturation electro-diffusion mechanisms acting between the diffuse layer and the bulk electrolyte controlled the low frequency response. This work provides valuable insight into dielectric polarisation mechanisms in shales, and demonstrates such measurements are sensitive to EDL properties and electro-diffusion length scales that are relevant to characterising pore properties in shales.

## 1 Introduction

The complex broadband (Hz to GHz) dielectric response of moist rocks arises from a range of polarisation processes related to individual molecules, interfacial charge phenomena and electrochemical potentials [1], [2]. Several authors have highlighted the potential of using electrical relaxation times to extract important hydraulic properties of rocks such as permeability [3], [4], textural properties of pore surfaces [5] and pore and pore throat sizes [6], [7]. However, despite many experimental studies [8] and theoretical considerations [9], a complete model for broadband dielectric polarisation in permeable rocks is still yet to be realised [10]. A limiting factor in this lack of physical insight is the widespread application of empirical models that are based on dielectric relaxation for a single dipole [11]–[13]. The alternative, and more physically appropriate approach, of fitting broadband dielectric dispersion data with a continuous distribution of relaxation times [14]–[16], of which there are only few examples in the literature that involved spectral induced polarisation measurements [17]–[19].

Here we demonstrate the successful application of Tikhonov regularisation methods to compute continuous distributions of dielectric relaxation times directly from

broadband (40 Hz – 110 MHz) frequency domain data for a shale rock at varied partial saturation. The evolution of dielectric relaxation distributions was studied as a function of water content, with measurements of 6 incremental saturation states ranging from dry to fully saturated. Analysis of the relaxation time distributions obtained as moisture content increased reveals new insights into the consequent changes in EDL polarisation processes. Furthermore, we attempt to quantify the contribution of in-phase conduction currents by using the inverted relaxation time distribution models and the Kramers-Kronig relation to link the solutions obtained for the real and imaginary components of the dielectric response.

## 2 Background and Theory

### 2.1 Effective Electrical Properties

In an applied electrical field ( $\vec{E}$ ), the effective current density ( $\vec{J}_E$ ) of a homogenous material is composed of two parts: conduction currents ( $\vec{J}_C$ ) and displacement currents ( $\vec{J}_D$ ),

\* Corresponding author: paul.connolly@uwa.edu.au

$$\vec{J}_E = \vec{J}_C + \vec{J}_D \quad (1)$$

where,

$$\vec{J}_C = \sigma \vec{E} \quad (2)$$

and,

$$\vec{J}_D = \varepsilon \frac{\partial \vec{E}}{\partial t} \quad (3)$$

Here  $\sigma$  is the electrical conductivity and  $\varepsilon$  the dielectric permittivity [20]. Conduction currents are defined as an ordered translation of free charge, which for rocks corresponds primarily to the translation of charge carrying ions present in fluids within the pore space. The magnitude of conduction is related to the charge, charge density and drift velocity [21] of the free charges being translated. Displacement currents relate to the time dependent polarisation processes of bound charges [22], which can occur from an atomic scale to macro assemblages of molecules. The extent of electrical polarisation is related to the density of effective dipoles, their polarizability and mobility.

In a time varying electrical field ( $\vec{E}$ ) with angular frequency  $\omega = 2\pi f$ , the relationship between the complex frequency dependence of conductance and displacement currents can be derived from Maxwell's equations [22],

$$\vec{J}_E(\omega) = \sigma^*(\omega)\vec{E} = \varepsilon^*(\omega) \frac{\partial \vec{E}}{\partial t} \quad (4)$$

where,

$$\varepsilon^*(\omega) = \left[ \varepsilon'(\omega) + \frac{\sigma''(\omega)}{\omega \varepsilon_0} \right] - i \left[ \varepsilon''(\omega) + \frac{\sigma'(\omega)}{\omega \varepsilon_0} \right] \quad (5)$$

and

$$\sigma^*(\omega) = [\sigma'(\omega) + \varepsilon''(\omega)\omega] + i[\sigma''(\omega) + \varepsilon'(\omega)\omega] \quad (6)$$

Here the effective dielectric permittivity ( $\varepsilon^*(\omega)$ ) The imaginary and real components of the permittivity ( $\varepsilon''(\omega)$ ) and conductivity ( $\sigma'(\omega)$ ) relate to ohmic conductance or the translation of charges, respectively, while real permittivity ( $\varepsilon'(\omega)$ ) and imaginary conductivity ( $\sigma''(\omega)$ ) components relate to the capacitive susceptance or the displacement of charges [20]. The measured electrical quantities  $\sigma^*(\omega)$  and  $\varepsilon^*(\omega)$  are in fact composites of complex conduction and polarisation processes. It is also useful to normalise  $\varepsilon^*(\omega)$  by the dielectric permittivity of free space  $\varepsilon_0$  and report the relative permittivities  $\varepsilon_r = \varepsilon^*/\varepsilon_0$ .

## 2.2 Dielectric Relaxation Time

For a single dipole, the frequency dependent complex dielectric permittivity,  $\varepsilon^*(\omega)$ , is given by the Debye model.

$$\varepsilon^*(\omega) - \varepsilon_\infty = \frac{\Delta\varepsilon}{1 + i\omega\tau} \quad (7)$$

Here  $\tau$  is the characteristic relaxation time,  $\varepsilon_\infty$  is dielectric permittivity at the high frequency limit and  $\Delta\varepsilon$  is the difference in permittivity between the high and low frequency limits. While the Debye model eloquently describes the response of a single dipole, heterogenous rocks represent complex and non-ideal dielectric systems where multiple dielectric processes occur because of strong surface-electrolyte charge interactions, highly varied compositions and complex pore structures. To better represent the ensemble of relaxation processes that occur in many complex dielectrics, the most widely used approach has been to empirically alter the exponential form of the Debye model by broadening [11] or combining broadening with functional asymmetry [13]. The Havriliak-Negami (HN) adaptation is one such model and takes the form,

$$\varepsilon^*(\omega) - \varepsilon_\infty = \frac{\Delta\varepsilon}{(1 + (i\omega\tau)^\alpha)^\beta} \quad (8)$$

where both  $\alpha$  and  $\beta$  are empirical fitting parameters ranging between 0 and 1. Note that if  $\beta$  is set to 1 the HN equation reduces to the Cole-Cole equation [11], and if  $\alpha$  is set to one it reduces to the Cole Davidson equation [12]. Although capable of fitting some complex dielectric data, the relationship of the values obtained for these empirical fitting parameters with physical processes is ambiguous. Furthermore, for broadband dielectric data covering frequency ranges that span many orders of magnitude, a combination of several such functions are usually required to fit the experimental data obtained, requiring a priori assumptions about the number of relaxation processes and approximate relaxation times[23]–[25].

Alternatively, broadband dielectric dispersion data can be described by a continuous distribution of Debye-like processes,

$$\frac{\varepsilon^*(\omega) - \varepsilon_\infty}{\Delta\varepsilon} = \int_{\tau_{\min}}^{\tau_{\max}} \frac{g(\tau)}{1 + i\omega\tau} d\tau \quad (9)$$

where  $g(\tau)$  represents the probability distribution of characteristic relaxation times. Analysis of the dielectric response data using this form provides distinct benefits over parametrised methods as dispersion processes can be assessed directly from relaxation time distributions. Numerically, however, this analysis is more difficult as the solution to the integral equation is ill-conditioned (i.e., many of the solutions for  $g(\tau)$  are linearly dependent and small changes in the signal can disproportionately impact the solution). One way to overcome the numerical problems associated with the ill-conditioned nature of the integral equation and to manage contributions of experimental noise is through the use regularisation methods, as developed for example by Tikhonov [26].

### 2.3 Dielectric Polarisation in Complex Materials

Dielectric dispersion observed in moist rocks arises from several polarisation mechanisms of effective dipoles that vary in mobility and size. At high electric field frequencies (>1 GHz) only small mobile dipoles, which typically correspond to individual molecules, and atomic and ionic structures can be polarised. As frequency is reduced, less mobile and larger effective dipoles related to restricted molecules, assemblages of molecules, and surface effects start contributing to the measured dielectric permittivity, as do electro-diffusion processes. Loewer et al. [23] provides a good overview and graphical representation of these polarisation mechanisms and their relationship to the frequency of applied electric field. Numerous models have been developed to describe electrical processes in rocks, which can be broadly divided into those derived from bulk properties [27]–[31] and those that incorporate surface related mechanisms (i.e. conduction and polarisation of surface charges) [1], [9], [32], [33].

Experimentally, Maxwell-Wagner-Bruggeman-Hanai (MWBH) theories have been shown to successfully describe experimental results well for most moist rocks at frequencies above 10 MHz [34]. However, at frequencies lower than this, contributions from surface processes to conduction and displacement currents can be much stronger than those accounted for by bulk effect models alone [35].

Surface polarisation and conduction models attempt to account for charged ions and effective dipoles, whose behaviour and assembled structure is defined by their interactions with an active surface. When a solid, charged surface is in contact with an ion-containing solution, an electrical double layer (EDL) will form in the vicinity of that surface. The EDL structure consists of tightly bound, immobile inner layer of ions with the opposite charge to that of the surface known as the Stern layer. Beyond the Stern layer, an ionic atmosphere called the diffuse layer is formed by ions of both charges, with a slightly higher concentration of those with the charge opposite to the surface [36].

O’Konski (1960) considered polarisation of charge carriers within an EDL moving tangentially along the surface of a spherical particle with radius  $a$ . In this approach, the surface conductivity ( $\sigma_s$ ) is considered to account for the mobility of charges in the EDL and displacement normal to the surface is not permitted. The relaxation time ( $\tau_s$ ) for establishing polarisation was hence derived,

$$\tau_s = \frac{a(\varepsilon_2 + 2\varepsilon_1)}{8\pi\sigma_s} \quad (10)$$

where  $\varepsilon_1$  and  $\varepsilon_2$  are the dielectric permittivities in the low frequency limit corresponding to the electrolyte and

particle respectively. Schwarz (1962) argued that O’Konski’s approach of expanding MW theory to include ohmic surface conductance around the particle was not enough to account for experimental observations, with dielectric permittivities many orders of magnitude higher than their constituents found for some composite materials. Instead, the relaxation time for polarisation in the EDL should be considered as controlled by the diffusion of surface bound ions ( $D_s$ ) [37],

$$\tau_s = \frac{a^2}{2D_s} \quad (11)$$

Comparisons of such models to experiments with suspensions of polystyrene spheres in an electrolyte solution showed improved agreement [32]. However, for polarisation in an time-dependent field, the surface ion diffusion interpretation is only valid in the limit of small particle size; for large particles the observed relaxation time is better described by the surface conductivity description [35]. Models which define the polarisation as occurring exclusively in the EDL (i.e. no interaction with the bulk electrolyte) are sometimes term *closed EDL* models [35]. Although applicable to a wide range of materials, these fixed layer models fail to capture the very large low frequency dielectric response observed in, for example, colloidal systems [38] and clay rich sands [39].

The boundary conditions of the *closed* double layer models can be altered to allow for diffusional flux of counter and co-ions from the EDL to the bulk electrolyte [37], [40], with the resulting formalism sometimes referred to as an *open* double layer model **Figure 1**. The driving force for this flux is a result of electrochemical potentials that arise between the bulk electrolyte and the distorted charge distribution of the polarised electrical double layer. These diffusive fluxes of ions can occur out of phase with the applied field and result in very large displacement currents, which is consistent with many experimental observations [39]. The characteristic relaxation times for these systems are also controlled by diffusion; however, in this case it is the bulk diffusion of counter and co-ions across a length scale  $a$ , which reflects the compositional front associated with the electrochemical potential,

$$\tau_D = \frac{a^2}{2D} \quad (12)$$

The exact dielectric polarisation mechanisms that occur in clay rich rocks are complex and likely to be a convolution of multiple different phenomena dependent on various length and time scales. Having a better fundamental understanding of the different polarisation process enables the interpretation of observed relaxation times in terms of various length scales. This in turn may lead to more accurate applications of dielectric relaxation time models to determine various key properties of rock samples that are otherwise difficult to determine.

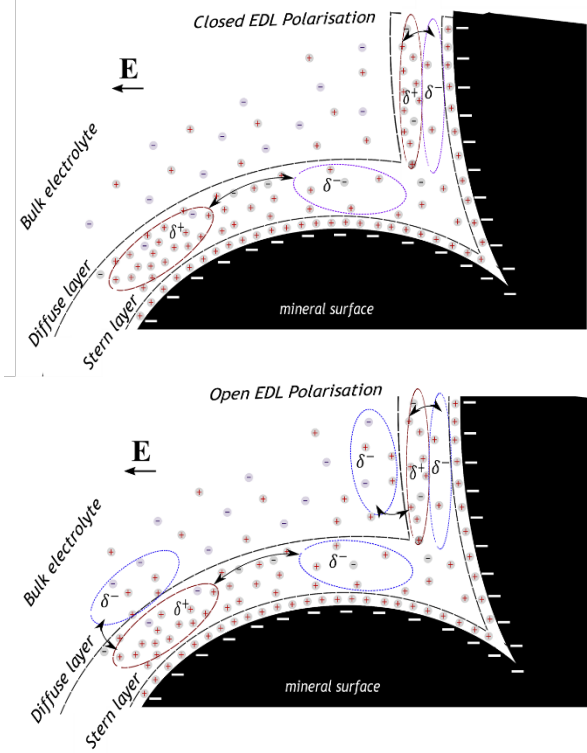


**Figure 1.** schematic of open and closed EDL polarisation processes. Arrows indicate charged ion transfer between positive and negative domains of effective dipoles.

## 3 Method

### 3.1 Samples

This study involved an American shale sample, which after acquisition from a well the sample was air dried, and thus still contained remnant formation salt. Dielectric measurements were made on a thin disc 8 mm thick and 25.4 mm in diameter which was cut from the original plug. The flat surfaces of the samples were cut with a tolerance of  $\pm 0.08$  mm.

**3.2 Saturation Protocol** The sample was measured at 6 saturation states ranging from dry to 100% saturated. First, the ‘as received’ shale sample was left in four different RH environments allowing for it to reach several different partial saturation states. Specifically, RH conditions of 99%, 75%, 43% and 23% were generated by placing saturated salt solutions of potassium sulfate, sodium chloride, potassium carbonate and potassium acetate, respectively, into temperature-controlled glass desiccators. The sample was removed periodically for weighing and equilibrium saturation was determined when the mass had stabilised to within approximately  $\pm 0.0005$  g; this process typically took 6 weeks. The effect of exposing shale to different RH environments was to vary its saturation state by the addition of pure H<sub>2</sub>O vapour, which effectively diluted or concentrated any electrolytes in the pore space.

Following this, the samples were placed under vacuum for 48 hrs and then pressure saturated (150 bar) with 1% NaCl solution, after which they were left for a

further 48 hrs at pressure. Finally, the samples were dried in a vacuum oven at 105°C for 3 weeks.

### 3.3 Dielectric Measurements

To remove the effects of ohmic conduction and electrode polarisation we made measurements with a regenerated cellulose sheet that acted as a blocking film in place between the sample and electrodes [41]. Repeat measurements were also made without the blocking film in place to record the equivalent conductivity. After each measurement the sample was rotated 180° and a repeat measurement was made, with the average of the two measurement reported here. Hence, a total of 24 individual test were conducted on this sample over the course of the experimental procedure.

At each saturation state, capacitance and resistance measurements were made using the three terminal parallel plate method, which includes the addition of a guarding electrode that minimises stray edge effects. Samples were placed in between the two platens (20 mm sensing diameter) with a small compression force applied using a manual hydraulic pump to ensure a firm surface contact. The dielectric measurement cell was connected to an Agilent 4294A impedance analyser which has a basic impedance accuracy of  $\pm 0.08\%$  and covers a broad frequency range of 40 Hz to 100 MHz. Parasitic capacitance contributions associated with the transmission lines and terminals were subtracted from the experimental data by conducting calibration measurements at the beginning of each experimental run.

### 3.4 Regularisation

To solve for  $g(\tau)$  from logarithmically spaced data we first introduce the following normalization condition,

$$\int_{\tau_{max}}^{\tau_{min}} g(\tau) d(\ln \tau) = 1 \quad (16)$$

Then, through the Kramers-Kronig relation, the measured real and imaginary components of the dielectric permittivity can be represented by a calculation based on a specified  $g(\tau)$ ,

$$\epsilon'_{(\omega)} = \epsilon_{\infty} + (\Delta\epsilon) \int_{\tau_{max}}^{\tau_{min}} \frac{g(\tau)}{1 + \omega^2\tau^2} d(\ln\tau) + s_n(\omega) \quad (17)$$

$$\epsilon''_{(\omega)} = (\Delta\epsilon) \int_{\tau_{max}}^{\tau_{min}} \frac{g(\tau)\omega\tau}{1 + \omega^2\tau^2} d(\ln\tau) + s_n(\omega) \quad (18)$$

Here  $s_n(\omega)$  is the noise associated with the experimental measurement. This more mathematically complex representation is a Fredholm integral of the first kind. The task then becomes to solve the inverse problem to determine  $g(\tau)$  from the measured complex dielectric permittivity. Regularisation methods, such as minimizing the residual norm, can be used to solve these Fredholm integrals for approximate solutions but discrete noisy signals can lead to unrealistic, highly oscillatory solutions. A well-established method for generating robust solutions for noisy data is Tikhonov regularisation

[26] where the minimisation quantity,  $H$ , is defined as [42],

$$H(\alpha) = \sum_j [\varepsilon_j^{exp} - \varepsilon_j^{est}]^2 + \alpha \|g(\tau)\| \quad (19)$$

where  $\varepsilon_j^{exp}$  are the experimental data,  $\varepsilon_j^{est}$  is the estimated solution and  $\alpha \|g(\tau)\|$  is the penalty term which balances the impact of noise to the fidelity of the final answer. The summation extends over both the real and imaginary components (i.e. contains  $2N$  elements where  $N$  is the number of frequencies at which  $\varepsilon_j^{exp}$  were measured). This method allows for the simultaneous regression real and imaginary data for a single  $g(\tau)$  solution. However, regression of a single  $N$  element (i.e. for either real or imaginary component only) is also easily implemented. Relaxation time models can then be translated between real and imaginary permittivity via the Kramer-Kronig relation.

In our implementation the penalty term is proportional to the second derivative of  $g(\tau)$  with respect to  $(\ln \tau)$ ,

$$\|g(\tau)\| = \int_D^0 [g''(\tau)]^2 d(\ln \tau) \quad (20)$$

The magnitude of the penalty term is governed by the smoothing coefficient  $\alpha$ . Translating this to matrix form we get,

$$H(\alpha) = |\mathbf{R}\mathbf{g} - \mathbf{b}|^2 + \alpha \|\mathbf{L}\mathbf{g}\| \quad (21)$$

$\mathbf{R}$  is the transfer matrix,  $\mathbf{g}$  is the probability distribution of dielectric relaxation times,  $\mathbf{b}$  is the measured signal inclusive of noise, and  $\|\mathbf{L}\mathbf{g}\|$  is the penalty term.

The selection of the smoothing parameter is an important step. If the magnitude of penalty function is too small then the solution appears under regularised, often highly oscillatory and generally unphysical. Conversely, if the penalty function is too large, then not enough weight is given to the exact analytical solution resulting in very broad, under-defined distributions [43]. To select the alpha value we have used an automated method of generalized cross validation (GCV), which is described in detail elsewhere [44]–[46]. The basis of the GCV method is to sequentially remove data from  $\mathbf{s}$  and determine which value of  $\alpha$  for the regularised solution best predicts the omitted data. Scores are assigned to a defined range of  $\alpha$  values, with the  $\alpha$  that minimizes the GCV score being the optimal smoothing parameter.

## 4 Results

**Figure 2** shows experimental data for the real and imaginary relative permittivity of the shale sample at the six saturation conditions measured. In the dry state, the real part of the dielectric response was relatively flat ranging from about 7 at 100 MHz to about 10 at 40 Hz. At the first RH condition (23%), at frequencies < 10 MHz,

the real part of the dielectric response rapidly increased to several hundred as frequency decreased to ~1 KHz, where a low frequency plateau was observed. In the high frequency range (10-100 MHz) the real part of the dielectric response began to converge toward a plateau. With increasing saturation the plateau in the low frequency region remained fairly constant, until at a critical saturation (typically occurring for samples exposed to greater than RH 75-99%) the real part of the dielectric response began to increase again at frequencies around 1 kHz and lower. At full saturation this effect was greatest, with some real relative permittivity values at 40 Hz reaching several tens of thousands for some samples. This low frequency transition to higher real permittivity as moisture content increased was coupled with a sharp increase in the imaginary component of the permittivity at sub-kHz frequencies.

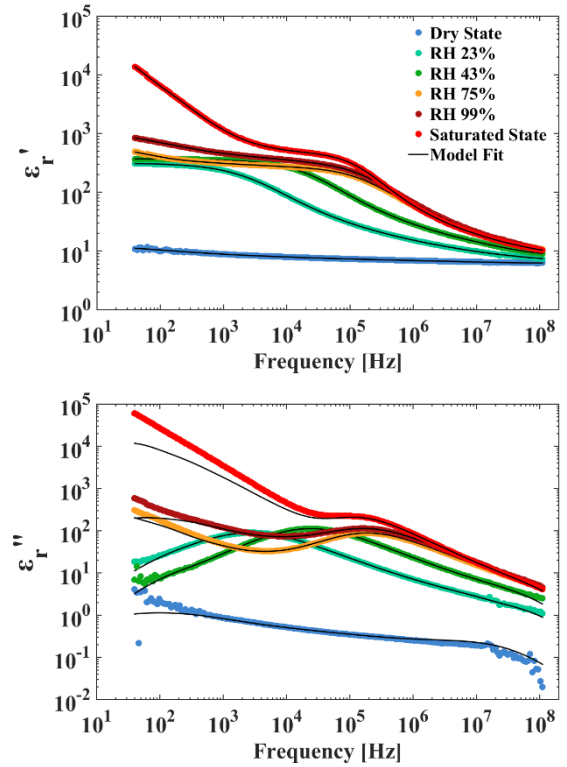


**Figure 2.** Measured real and imaginary dielectric permittivity of shale sample at varied saturation conditions. The real permittivity is fitted with the  $g(\tau)$  regularised solutions (Model fit). The imaginary data is compared against the equivalent KK model derived from the real permittivity  $g(\tau)$  solution.

Using the regularisation steps previously outlined, we minimise a solution of  $g(\tau)$  against the real permittivity data (i.e.  $\varepsilon'_{(\omega)}$  only). Then, via the Kramers-Kronig relation we generate the model solution,  $\varepsilon''_{(\omega)}^{(KK)}$ , for the imaginary component of the permittivity using the  $g(\tau)$  solution derived from on the real part of the permittivity data. This model solution,  $\varepsilon''_{(\omega)}^{(KK)}$ , is then compared against the measured values for the imaginary permittivity (i.e.  $\varepsilon''_{(\omega)}$ ) (**Figure 2**). Assuming  $\frac{\sigma'_{(\omega)}}{\omega\varepsilon_0} \gg \frac{\sigma''_{(\omega)}}{\omega\varepsilon_0}$ , which to a first order approximation should be true at frequencies < 1 MHz, then the differences between

$\varepsilon''(\omega)^{(KK)}$  and the experimental data will be related to in phase conduction current (equation 5). By subtracting the difference between  $g(\tau)$  and the imaginary data, the in phase conduction at low frequency could be quantified **Figure 3**.

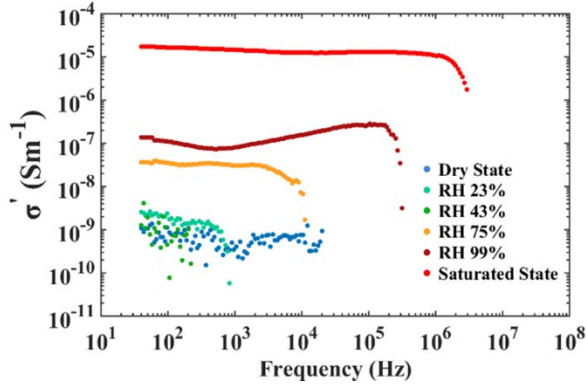


**Figure 3.** Values of  $\sigma'$  extracted from the differences between  $g(\tau)$  solutions from real component of the dielectric permittivity and imaginary permittivity data plotted as function of frequency.

The increase in a sample's moisture content driven by humidity produced negligible contributions to in-phase conductivity up to a RH of 45%. At higher values of RH, conduction increased appreciably at frequencies below a critical value which also increased with moisture content. Above RH 45 %, the conduction magnitude increased appreciably with each increment in moisture content and was largely independent of frequency. We suspect the observed onset of conduction arises from counter diffusion currents between the bulk electrolyte and the polarised diffuse layer within the EDL (open EDL). In this case, the electrochemical potential that results from a deformed EDL drives the mass diffusion of ions as the system moves to electro-neutrality [47]. The magnitude of the conduction relates to the number of charge carriers involved, and the critical frequency to the electrostatic activation energy a charge carrier needs to overcome to exchange from the diffuse layer to the bulk (i.e. when EDL counterion diffusivity > time EDL is polarised).

The evolution of dielectric relaxation time distributions with increasing moisture are shown in **Figure 4**. At the lowest RH condition (23%), the magnitude of  $\Delta\varepsilon$  dramatically increased and the dominant relaxation time observed ranged from  $10^{-3} - 10^{-4}$  s. Subsequent increases in moisture resulted in a downward shift of the dominant relaxation time, while the magnitude of  $\Delta\varepsilon$  contribute by this polarisation process remained relatively constant. This observation is better described by the phenomenological model for EDL polarisation [32], [48] than by a MW-type polarisation. Increased water vapour saturation will result in a decrease in charge concentration, which in turn will result in the expansion of diffuse part of the EDL [36] and an increase in the counterion diffusivity [49]. From numerical studies of the Debye- Falkenhagen dynamics, a decrease in charge density would result in an increased characteristic

relaxation time (opposite to that observed) while an increased counterion diffusivity would reduce the apparent relaxation time [50]. Hence, our experimental results suggest that the increased diffusivity of charge carriers in the EDL is the controlling factor in the observed shift in relaxation times between  $10^{-3}$ - $10^{-6}$  s. The relatively constant magnitude of  $\Delta\varepsilon$  suggests that for relative humidities between 23% and 45%, the polarisation process is constrained to within the EDL (i.e. a closed EDL with no exchange to the bulk).

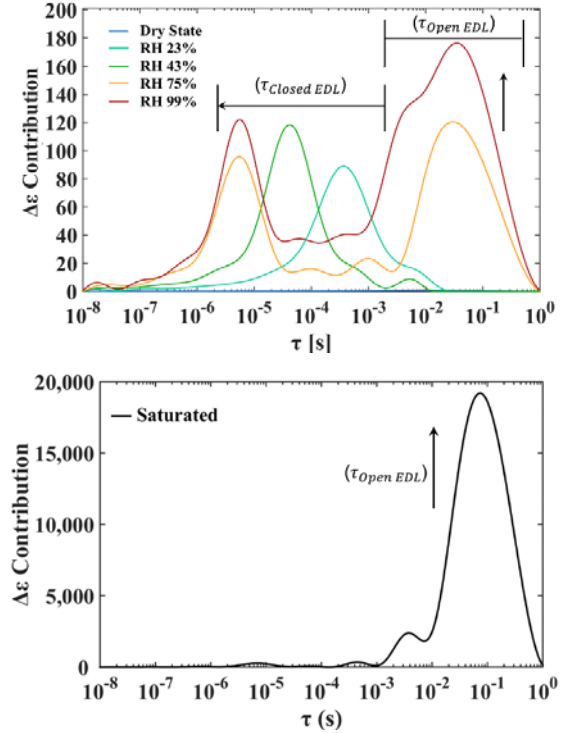


**Figure 4.** Evolution of dielectric relaxation time distributions after exposure to different RH environments. Domains with dominate polarisation mechanisms closed electrical double layer ( $\tau_{closed\ EDL}$ ) and open electrical double or diffusion fluxes ( $\tau_{open\ EDL}$ ) are identified. Arrows indicate trend with increasing saturation. The  $\Delta\varepsilon$  contribution from  $\tau_{open\ EDL}$  for the fully saturated states is much larger and hence it has been presented separately for clarity.

At around the saturation state incurred at RH 75% there was a sharp increase in  $\Delta\varepsilon$  that is related to a polarisation process with characteristic relaxation times  $\sim 10^{-2}$ - $10^{-1}$  s. Furthermore, at a fully saturated conditions this polarisation mechanism completely dominates (**Figure 4**). This very large low frequency dielectric response is consistent with *open* EDL polarisation (often referred to as membrane polarisation) where a coupled electro-diffusional mechanism is acting between the diffuse part of the EDL and the bulk electrolyte, giving rise to large in-phase displacement currents and slow relaxation times ( $\tau_D$ ) [39]. This polarisation mechanism is driven by the difference in electrochemical potential between a polarised EDL and the bulk, which causes diffusive fluxes of oppositely charged ions.

## 5 Conclusion

Here we demonstrate the application of Tikhonov regularisation methods to compute dielectric relaxation time distributions from broadband (40Hz to 110MHz) dielectric data for a shale sample at varying partial saturation. The evolution in the dielectric response with moisture content was driven by polarization processes within the EDL (closed EDL) up to an apparent critical partial saturation. Thereafter, the polarisation was dominated by diffusion between the EDL and the bulk electrolyte (open EDL). Future work will extend the analysis such that the relaxation time analysis can be readily converted into diffusion lengths, hence allowing for microstructure quantification. Furthermore, including a greater range of measurement frequencies (i.e. mHz – Hz and GHz) will assist in developing complete electrical property models for rocks and will also be a focus of future work.

## References

1. R. Knight *et al.*, “Geophysics At the Interface : Response of Geophysical Properties To Solid - Fluid , Fluid - Fluid , and Solid - Solid Interfaces,” *Rev. Geophys.*, vol. 48, no. 2007, pp. 1–30, 2010.
2. D. P. Lesmes and F. D. Morgan, “Dielectric spectroscopy of sedimentary rocks,” *J. Geophys. Res. Earth*, vol. 106, no. B7, pp. 13329–13346, 2001.
3. K. Titov, A. Tarasov, Y. Ilyin, N. Seleznev, and A. Boyd, “Relationships between induced polarization relaxation time and hydraulic properties of sandstone,” *Geophys. J. Int.*, vol. 180, no. 3, pp. 1095–1106, 2010.
4. A. Revil and N. Florsch, “Determination of permeability from spectral induced polarization in granular media,” *Geophys. J. Int.*, vol. 181, no. 3, pp. 1480–1498, 2010.
5. W. E. Kenyon, “Texture effects on megahertz dielectric properties of calcite rock samples,” *J. Appl. Phys.*, vol. 55, no. 8, pp. 3153–3159, 1984.
6. G. Osterman, K. Keating, A. Binley, and L. Slater, “A laboratory study to estimate pore geometric parameters of sandstones using complex conductivity and nuclear magnetic resonance for permeability prediction,” *Water Resour. Res.*, vol. 52, pp. 4321–4337, 2016.
7. A. Revil, “Effective conductivity and permittivity of unsaturated porous materials in the frequency range 1 mHz-1GHz,” *Water Resour. Res.*, vol. 49, no. 1, pp. 306–327, 2013.
8. R. D. Swanson *et al.*, “Anomalous solute transport in saturated porous media: Relating transport model parameters to electrical and nuclear magnetic resonance properties,” *Water Resour. Res.*, vol. 51, pp. 1264–1283, 2015.
9. A. Revil and P. Leroy, “Constitutive equations for ionic transport in porous shales,” *J. Geophys. Res.*, vol. 109, no. B3, p. B03208, 2004.
10. A. Binley, S. Kruschwitz, D. Lesmes, and N. Kettridge, “Exploiting the temperature effects on low frequency electrical spectra of sandstone: A comparison of effective diffusion path lengths,” *Geophysics*, vol. 75, no. 6, pp. A43–A46, 2010.
11. K. S. Cole and R. H. Cole, “Dispersion and absorption in dielectrics I. Alternating current characteristics,” *J. Chem. Phys.*, vol. 9, no. 4, pp. 341–351, 1941.
12. D. W. Davidson and R. H. Cole, “Dielectric relaxation in glycerol, propylene glycol, and n-propanol,” *J. Chem. Phys.*, vol. 19, no. 12, pp. 1484–1490, 1951.
13. S. Havriliak and S. Negami, “A complex plane analysis of  $\alpha$ -dispersions in some polymer systems,” *J. Polym. Sci. Part C Polym. Symp.*, vol. 14, no. 1, pp. 99–117, 1966.
14. S. M. Usmanov, “Use of the tikhonov regularization method in automated mathematical analysis of dielectric spectrometry data,” *Sov. Phys. J.*, vol. 34, no. 10, pp. 931–936, 1990.
15. F. D. Morgan and D. P. Lesmes, “Inversion for dielectric relaxation spectra,” *J. Chem. Phys.*, vol. 100, no. 1, pp. 671–681, 1994.
16. H. Schäfer, E. Sternin, R. Stannarius, M. Arndt, and F. Kremer, “Novel approach to the analysis of broadband dielectric spectra,” *Phys. Rev. Lett.*, vol. 76, no. 12, pp. 2177–2180, 1996.
17. A. Tarasov and K. Titov, “Relaxation time distribution from time domain induced polarization measurements,” *Geophys. J. Int.*, vol. 170, no. 1, pp. 31–43, 2007.
18. S. Nordsiek and A. Weller, “A new approach to fitting induced-polarization spectra,” *Geophysics*, vol. 73, no. 6, p. F235, 2008.
19. M. Tong, L. Li, W. Wang, and Y. Jiang, “Determining capillary-pressure curve, pore-size distribution, and permeability from induced polarization of shaley sand,” *Geophysics*, vol. 71, no. 3, p. N33, 2006.
20. N. Wagner, K. Emmerich, F. Bonitz, and K. Kupfer, “Experimental Investigations on the Frequency- and Temperature-Dependent Dielectric Material Properties of Soil,” *Ieee Trans. Geosci. Remote Sens.*, vol. 49, no. 7, pp. 2518–2530, 2011.
21. A. Revil and P. Glover, “Theory of ionic-surface electrical conduction in porous media,” *Phys. Rev. B - Condens. Matter Mater. Phys.*, vol. 55, no. 3, pp. 1757–1773, 1997.
22. B. D. Fuller and S. H. Ward, “Linear System Description of the Electrical Parameters of Rocks,” *IEEE Trans. Geosci. Electron.*, vol. 8, no. 1, pp. 7–18, 1970.
23. M. Loewer, T. Günther, J. Igel, S. Kruschwitz, T. Martin, and N. Wagner, “Ultra-broad-band electrical spectroscopy of soils and sediments—a combined permittivity and conductivity model,” *Geophys. J. Int.*, vol. 210, no. 3, pp. 1360–1373, 2017.
24. D. P. Lesmes and F. D. Morgan, “Dielectric spectroscopy of sedimentary rocks,” *J. Geophys. Res. Solid Earth*, vol. 106, no. B7, pp. 13329–13346, 2001.

25. G. Goracci, M. Monasterio, H. Jansson, and S. Cervený, "Dynamics of nano-confined water in Portland cement - Comparison with synthetic C-S-H gel and other silicate materials," *Sci. Rep.*, vol. 7, no. 1, pp. 1–10, 2017.
26. A. N. Tikhonov, "Solution of Incorrectly Formulated Problems and the Regularisation Method.pdf," *Sov. Math. Dokl.*, vol. 4, no. 4, pp. 1035–1038, 1963.
27. J. C. Maxwell, *A treatise on electricity and magnetism*. New York: Dover Publ. Inc., 1891.
28. K. W. Wagner, "Erklärung der Dielectricischen Nachwirkungsvorgänge auf grund Maxwell'scher vorstellungen," *Arch. Electrotech.*, vol. 2, pp. 371–381, 1924.
29. D. Bruggeman, "Berechnung Verschiedener Physikalischer Konstanten von Heterogenen Substanzen," *Ann. Phys.*, vol. 24, pp. 636–679, 1935.
30. R. W. Sillars, "The properties of a dielectric containing semiconducting particles of various shapes," *Inst. Electr. Eng. - Proc. Wirel. Sect. Inst.*, vol. 12, no. 35, pp. 139–155, 1937.
31. T. Hanai, "Dielectric properties of emulsions IV. Dielectric Behavior of Nitrobenzene-in Water Emulsions," *Kolloid-Zeitschrift*, vol. 184, no. 2, pp. 143–148, 1962.
32. G. Schwarz, "A Theory of the Low-Frequency Dielectric Dispersion of Colloidal Particles in Electrolyte Solution," *J. Phys. Chem.*, vol. 66, no. 12, pp. 2636–2642, 2007.
33. C. T. O'Konski, "Electric properties of macromolecules. V. Theory of ionic polarization in polyelectrolytes," *J. Phys. Chem.*, vol. 64, no. 5, pp. 605–619, 1960.
34. T. L. Chelidze, Y. Guéguen, and C. Ruffet, "Electrical spectroscopy of porous rocks: a review- II. Experimental results and interpretation," *Geophys J Int*, vol. 137, no. August, pp. 16–34, 1999.
35. T. L. Chelidze and Y. Guéguen, "Electrical spectroscopy of porous rocks: a review- I. Theoretical models," *Geophys J Int*, vol. 137, no. April, pp. 1–15, 1999.
36. H. L. Bohn and B. L. Mcneal, "A qualitative derivation of the diffuse double layer 1," *J. Agron. Educ.*, vol. 12, p. 2628, 1983.
37. S. S. Dukhin and V. N. Shilov, *Dielectric Phenomena and Double Layer in Disperse Systems and Polyelectrolytes*. New York: John Wiley & Sons, 1974.
38. L. A. Rosen, J. C. Baygents, and D. A. Saville, "The interpretation of dielectric response measurements on colloidal dispersions using the dynamic Stern layer model," *J. Chem. Phys.*, vol. 98, no. 5, pp. 4183–4194, 1993.
39. O. De Lima and M. Sharma, "A generalized Maxwell-Wagner theory for membrane polarization in shaly sands," *Geophysics*, vol. 57, no. 3, pp. 431–440, 1992.
40. M. Fixman, "Charged macromolecules in external fields . I . The sphere," vol. 5177, no. 1980, 1993.
41. M. Josh, B. Clennell, M. Cauchefert, and T. Han, "Dielectric permittivity and anisotropy of intact multi-saturated organic shales," *SPWLA 57 th Annu. Logging Symp. June 25 - 29*, no. June, p. 14, 2016.
42. B.-G. Kim and J.-J. Kim, "Application of tikhonov regularization to dipole glass relaxation function," *Ferroelectrics*, vol. 206, no. 1, pp. 79–91, 1998.
43. P. R. J. Connolly, S. J. Vogt, S. Iglauer, E. F. May, and M. L. Johns, "Capillary trapping quantification in sandstones using NMR relaxometry," *Water Resour. Res.*, pp. 1–16, 2017.
44. G. Wahba, "Practical Approximate Solutions to Linear Operator Equations When the Data are Noisy," *SIAM Journal on Numerical Analysis*, vol. 14, no. 4, pp. 651–667, 1977.
45. J. D. Wilson, "Statistical approach to the solution of first-kind integral equations arising in the study of materials and their properties," *J. Mater. Sci.*, vol. 27, no. 14, pp. 3911–3924, 1992.
46. K. G. Hollingsworth and M. L. Johns, "Measurement of emulsion droplet sizes using PFG NMR and regularization methods," *J. Colloid Interface Sci.*, vol. 258, no. 2, pp. 383–389, 2003.
47. V. N. Shilov, A. V. Delgado, F. Gonz, and J. Horno, "Polarization of the Electrical Double Layer . Time Evolution after Application of an Electric Field," *J. Colloid Interface Sci.*, vol. 148, pp. 141–148, 2000.
48. J. M. Schurr, "On the Theory of the Dielectric Dispersion of Spherical Colloidal Particles in Electrolyte Solution1," *J. Phys. Chem.*, vol. 68, no. 9, 1964.
49. I. C. Bourg and G. Sposito, "Molecular dynamics simulations of the electrical double layer on smectite surfaces contacting concentrated mixed electrolyte (NaCl – CaCl<sub>2</sub>) solutions," *J. Colloid Interface Sci.*, vol. 360, no. 2, pp. 701–715, 2011.
50. M. B. Singh and R. Kant, "Debye-Falkenhagen dynamics of electric double layer in presence of electrode heterogeneities," *J. Electroanal. Chem.*, vol. 704, pp. 197–207, 2013.